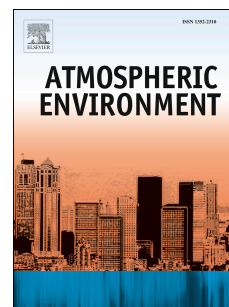| Title	Gas- and particle-phase products from the photooxidation of acenaphthene and acenaphthylene by OH radicals
Authors	Riva, Matthieu;Healy, Robert M.;Flaud, Pierre-Marie;Perraudin, Emilie;Wenger, John C.;Villenave, Eric
Publication date	2017-11-30
Original Citation	Riva, M., Healy, R. M., Flaud, P.-M., Perraudin, E., Wenger, J. C. and Villenave, E. (2017) 'Gas- and particle-phase products from the photooxidation of acenaphthene and acenaphthylene by OH radicals', Atmospheric Environment, 151, pp. 34-44. doi:10.1016/j.atmosenv.2016.11.063
Type of publication	Article (peer-reviewed)
Link to publisher's version	10.1016/j.atmosenv.2016.11.063
Rights	© 2016 Elsevier Ltd. This manuscript version is made available under the CC-BY-NC-ND 4.0 license - http://creativecommons.org/licenses/by-nc-nd/4.0/
Download date	2025-07-30 10:57:23
Item downloaded from	https://hdl.handle.net/10468/3554

Accepted Manuscript

Gas- and particle-phase products from the photooxidation of acenaphthene and acenaphthylene by OH radicals

Matthieu Riva, Robert M. Healy, Pierre-Marie Flaud, Emilie Perraudin, John C. Wenger, Eric Villenave

Please cite this article as: Riva, M., Healy, R.M., Flaud, P.-M., Perraudin, E., Wenger, J.C., Villenave, E., Gas- and particle-phase products from the photooxidation of acenaphthene and acenaphthylene by OH radicals, *Atmospheric Environment* (2016), doi: 10.1016/j.atmosenv.2016.11.063.

Gas- and particle-phase products from the photooxidation of acenaphthene and acenaphthylene by OH radicals

Matthieu Riva,[†,‡,#] Robert M. Healy,[§,¥] Pierre-Marie Flaud,[†,‡] Emilie Perraudin,[†,‡] John C. Wenger,[,§] Eric Villenave [*,†,‡]*

† Univ. Bordeaux, EPOC, UMR 5805, F-33405 Talence cedex, France

‡ CNRS, EPOC, UMR 5805, F-33405 Talence cedex, France

§ Department of Chemistry and Environmental Research Institute, University College Cork, Cork, Ireland

Now at the Department of Physics, PO Box 64, 00014 University of Helsinki, Finland

¥ Now at Environmental Monitoring and Reporting Branch, Ontario Ministry of the Environment and Climate Change, Toronto, Canada

* Corresponding Authors:

     Email - e.villenave@epoc.u-bordeaux1.fr; Phone – 33-5-4000-6350

     Email - j.wenger@ucc.ie; Phone – 353-2-1490-2454

Abstract

This work is focused on the gas-phase oxidation of acenaphthylene and acenaphthene by OH radicals and associated secondary organic aerosol (SOA) formation under low and high-NO_x conditions. Experiments were carried out in an atmospheric simulation chamber using a proton transfer reaction time-of-flight-mass spectrometer (PTR-TOF-MS) and an aerosol time-of-flight-mass spectrometer (ATOFMS) to chemically characterize the gas- and particle-phase products, respectively. Due to the structures of these two aromatic compounds, the proposed chemical mechanisms exhibit some differences. In the case of acenaphthene, H-atom abstraction from the saturated cyclopenta-fused ring was found to be competitive with the OH-addition to the aromatic rings. During the photooxidation of acenaphthene using nitrous acid (HONO), aromatic ring-opening products such as indanone and indanone carbaldehyde, generated through OH addition to the aromatic ring, were formed in higher yields compared to low-NO_x conditions. In the case of acenaphthylene, OH addition to the unsaturated cyclopenta-fused ring was strongly favored. Hence, ring-retaining species such as acenaphthenone and acenaphthenequinone, were identified as the main reaction products in both gas- and particle-phases, especially under high-NO_x conditions. Subsequent SOA formation was observed in all experiments and SOA yields were determined under low/high-NO_x conditions to be 0.61/0.46 and 0.68/0.55 from the OH-initiated oxidation of acenaphthylene and acenaphthene, respectively.

1. Introduction

Atmospheric fine particulate matter (PM$_{2.5}$, aerosol with aerodynamic diameters less than 2.5 µm) plays a key role in air quality and climate change, and is associated with damaging effects on human health (Pope III and Docherty, 2006; Hallquist et al., 2009). Globally, the largest mass fraction of PM$_{2.5}$ is organic (up to 90% in some locations) and is dominated by secondary organic aerosol (SOA). Formation of SOA mainly results from the formation of gas-phase products with low vapor pressures from the oxidation of volatile organic compounds (VOCs) (Hallquist et al., 2009). The anthropogenic contribution to global SOA formation is estimated to be small, actually around 10% (Kroll et al., 2008). SOA formation from anthropogenic sources is, however, suggested to be higher than currently predicted (Volkamer et al., 2006; Hallquist et al., 2009). In order to explain the current discrepancy between the mass of aerosols measured in different atmospheres and the mass predicted by atmospheric models, some studies have suggested that other sources of SOA are not yet identified or well characterized (Kroll et al., 2008; Hallquist et al., 2009). Among them, heterogeneous chemistry (formation of oligomers and organosulfates) (Surratt et al., 2008; Pye and Pouliot, 2012) and the contribution of intermediate volatility organic compounds (IVOCs) to SOA formation have been proposed (Robinson et al., 2007; Tkacik et al., 2012). It is worth noting that recent studies have also underlined that reactive uptake and/or multiphase chemistry of water-soluble volatile organic compounds, such as glyoxal, in wet acidic aerosols or cloud droplets could be an important source of SOA (Galloway et al., 2009; Ervens et al., 2011; Pye et al., 2013; Marais et al., 2016). Nevertheless, a large part of the underestimation in urban areas, due to the non-considered IVOC contribution to SOA formation, comes from the involvement of alkanes and polycyclic aromatic hydrocarbons (PAHs) (Tkacik et al., 2012). Much of the current efforts in the research community are focused on trying to identify these missing or misrepresented SOA sources.

PAHs are emitted into the atmosphere from incomplete combustion processes of organic materials and have been identified as major components in traffic and wood burning emissions. The PAHs with less than four aromatic rings exist mainly in the gaseous phase and can undergo photooxidation processes with different atmospheric oxidants (Atkinson and Aschmann, 1988; Sasaki et al., 1998; Keyte et al., 2013; Zhou and Wenger, 2013a,b; Riva et al., 2014). When oxidized, these compounds have been shown to produce large range of oxygenated and nitro compounds with high molecular weights (Sasaki et al., 1998; Reisen and

72 Arey, 2002; Lee and Lane, 2009; Kautzman et al., 2010; Kleindienst et al., 2012; Zhou et al.,

73 2013a,b; Riva et al., 2015a,b,c, 2016). Although PAHs are potentially carcinogenic and

74 mutagenic (Atkinson and Arey, 1994) some of their oxidation products present a larger

75 toxicity than their parent hydrocarbons (Lin et al., 2005). Gas-phase products can partition to

76 the particle phase and participate in SOA formation (Chan et al., 2009; Kautzman et al., 2010;

77 Shakya et al., 2010; Kleindienst et al., 2012; Riva et al., 2015a; Chen et al., 2016; Riva et al.,

78 2016). A few studies have previously reported the importance of naphthalene gas phase

79 photooxidation in SOA formation (Chan et al., 2009; Kleindienst et al., 2012). Other gaseous

80 PAHs have, however received less attention. Acenaphthylene and acenaphthene are fairly

81 unique among PAHs in that they contain a carbon-carbon double bond and a saturated carbon-

82 carbon bond, respectively, in their structure that enables them to react quickly with all

83 atmospheric oxidants including OH and NO_3 radicals, Cl atoms and O_3 (Atkinson and

84 Aschmann, 1988; Reisen and Arey, 2002; Zhou and Wenger, 2013a,b; Riva et al., 2014).

85 Acenaphthylene and acenaphthene were identified in both indoor and outdoor atmospheres

86 and in large concentrations in certain areas (Chang et al., 2006; Ho et al., 2009). The

87 concentration of both PAHs (greater than 20-30 ng m^{-3}) could be even comparable to that of

88 naphthalene in certain urban atmospheres (Dejean et al., 2009; Hanedar et al., 2014)

89 suggesting that acenaphthylene and acenaphthene might contribute to SOA formation in such

90 areas. Large rate constants for the reaction of acenaphthene ($(7.69 \pm 1.91) \times 10^{-11}$) and

91 acenaphthylene ($(1.14 \pm 0.08) \times 10^{-10}$) in cm^3 molecule^{-1} s^{-1}) with OH radicals have been

92 previously reported (Atkinson and Aschmann, 1988; Zhou and Wenger, 2013a,b). These

93 previous efforts underline the potential importance of the OH initiated oxidation of

94 acenaphthylene and acenaphthene in the atmospheric chemistry of PAHs. Indeed, it has been

95 shown that the reactivity of aromatic hydrocarbons is dominated by their reactions with the

96 OH radicals in the atmosphere (Calvert et al., 2002; Estève et al., 2003; Atkinson and Arey,

97 2007). Although the OH-initiated oxidation of PAHs has been studied previously, the impact

98 of NO_x concentration on the reactivity of PAHs remains poorly documented. Only two studies

99 on the oxidation of naphthalene performed under high- and low-NO_x conditions, have been

100 reported hitherto (Kautzman et al., 2009; Kleindienst et al., 2012). Previous works have

101 determined the rate constants and oxidation products for the photooxidation of acenaphthene

102 and acenaphthylene in the presence of NO_x (Atkinson and Aschmann, 1988; Reisen and Arey,

103 2002; Zhou and Wenger, 2013a,b). In addition, Shakya and Griffin (2010) have, for the first

104 time, reported the SOA yields arising from these reactions. These results highlight the

105 propensity for both PAHs to participate in SOA formation and only partial mechanisms were

4

106 proposed in these previous studies. However, some discrepancies remain and further work is

107 needed to clarify the reaction products as well as the chemical mechanisms leading to SOA

108 formation.

109 In this work, we performed a series of simulation chamber experiments to identify products

110 arising from the photooxidation of acenaphthylene and acenaphthene under low- and high-

111 NO_x conditions using state-of-the-art mass spectrometry techniques for on-line analysis of

112 both gaseous (proton transfer reaction time-of-flight-mass spectrometer) and particulate

113 (aerosol time-of-flight-mass spectrometer) phases. Based on these approaches, extended and

114 improved reaction mechanisms for the OH-initiated oxidation of acenaphthylene and

115 acenaphthene are now proposed. SOA growth and yields are determined in both cases to

116 evaluate the importance of the photooxidation of acenaphthene and acenaphthylene in SOA

117 formation.

118

119 2. Experimental section

120 Experiments were performed at room temperature (293 ± 2 K) and atmospheric pressure in

121 the 3910 L atmospheric simulation chamber at University College Cork, which is described in

122 detail elsewhere (Thüner et al., 2004). Briefly, it is a cylinder consisting of a Teflon FEP foil

123 tube closed with aluminum plates covered with Teflon FEP foil. The chamber is equipped

124 with fans to ensure rapid mixing of reactants and is surrounded by 16 lamps (Philips TL12,

125 40W) with an emission maximum at 310 nm and 12 lamps (Philips TL05, 40 W) with an

126 emission maximum at 360 nm (Kourtchev et al., 2009). Before each experiment, the chamber

127 is cleaned by flushing with dried purified air and photolysis of added ozone (ca. 1 ppmv) until

128 the particle number concentration is below 200 cm^{-3}. The flushing also reduces the levels of

129 NO_x and non-methane hydrocarbons to < 10 ppbv. The mixing ratios of NO_x and O_3 are

130 measured using standard automated gas analyzers (Thermo Model 42i and 49i respectively).

131 The temperature and water concentration in the chamber were monitored by a dew point

132 meter (Vaisala DM70). The relative humidity in the chamber was typically less than 1% for

133 the experiments with HONO and less than 5% for experiments carried out with H_2O_2.

134

135 Acenaphthylene (Sigma-Aldrich, 99%) and acenaphthene (Sigma-Aldrich, 99%) were

136 introduced into the chamber by flowing dry purified air throughout a heated Pyrex glass bulb

137 containing a known amount of the solid compound sufficient to produce PAH mixing ratios

138 around 300 ppb (Table S1). The PAHs and gas-phase oxidation products were monitored

5

139   during the experiments using a proton transfer reaction - time of flight - mass spectrometer

140   (PTR-TOF-MS, Kore Technology Ltd.). Details of the instrument and its operating principle

141   are given in Cappelin et al. (2012). Briefly, H_3O^+ is produced in a hollow cathode ion source

142   and reacts with organic compounds (M) that have a higher proton affinity than H_2O to

143   generate positively charged ions $(M + H)^+$, which are subsequently detected using a time-of-

144   flight mass spectrometer. The PTR-TOF-MS was operated over the m/z range 0-300 using a

145   sampling time of 1 min. The decay of the PAHs was monitored by following the protonated

146   molecular ions: m/z 153 (acenaphthylene) and m/z 155 (acenaphthene). Quantification of

147   identified products was not possible due to difficulty obtaining accurate concentrations in the

148   gas phase during the PTR-TOF-MS calibration.

149

150   Experiments were carried out in order to study the oxidation of acenaphthylene and

151   acenaphthene under high- and low-NO_x conditions. Nitrous acid (HONO) was used as an OH

152   radical precursor and was generated by adding 0.5 mL of 1 wt % aqueous sodium nitrite

153   ($NaNO_2$, Sigma-Aldrich, 97%) dropwise into 30 mL of 30 wt % sulfuric acid (Sigma-Aldrich,

154   99.9%) in a glass bulb (Cox, 1974). Purified air was flowed through the bulb, delivering

155   HONO to the chamber. The injection of HONO was stopped when the concentration of

156   nitrogen dioxide reached about 200 ppb in the chamber. Hydrogen peroxide (H_2O_2, Sigma-

157   Aldrich, 50 wt %) was used to generate OH radicals without NO_x. 60 µL was injected into the

158   glass bulb followed by slight heating. Purified air was passed through the bulb to introduce

159   H_2O_2 into the chamber.

160

161   The formation and growth of SOA was monitored using a scanning mobility particle sizer

162   (SMPS, TSI model 3034): size distribution, number and mass concentrations were determined

163   for all experiments, assuming an SOA density of 1.4 g cm^{-3} (Chan et al., 2009; Shakya et al.,

164   2010). SOA chemical composition was investigated using an aerosol time-of-flight mass

165   spectrometer (ATOFMS, TSI model 3800), which has been described in detail elsewhere

166   (Gard et al., 1997). Briefly, single particles are sampled through a critical orifice and focused

167   into a tight beam in the aerodynamic lens before transmission to the sizing region. The

168   velocity of the particles is measured using two continuous wave diode-pumped Nd:YAG

169   lasers operating at 532 nm. The time between these two scattering events is used to obtain the

170   aerodynamic size. Aerosols are then transmitted to the ionization region of the instrument

171   where desorption/ionization is performed by a Nd:YAG laser at 266 nm. This ablation process

172   generates high densities of charges, in which intermolecular interactions and matrix effects

6

173   often determine the ion distribution, making quantitative calibration of mass spectra

174   extremely difficult (Zelenyuk and Imre, 2005). Due to instrumental issues only positive ions

175   were detected using the ATOFMS. It is important to note, however, that PAHs are mainly

176   detected as positive ions (Silva and Prather, 2000; Zimmermann et al., 2003). The laser is

177   typically operated with an output energy of around 1 mJ per pulse. However, as described

178   elsewhere lower pulse energies were used in this work to reduce fragmentation of the organic

179   constituents in the aerosol (Zimmermann et al., 2003; Gross et al., 2000; 2005).

180

181   Based on the measured decay of PAH and known rate constants for reaction with OH (unit:

182   cm^3 molecule^{-1} s^{-1}): $(7.69 \pm 1.91) \times 10^{-11}$ and $(1.14 \pm 0.08) \times 10^{-10}$ for acenaphthene and

183   acenaphthylene, respectively (Atkinson and Aschmann, 1988; Brubaker and Hites, 1998;

184   Banceau et al., 2001; Reisen and Arey, 2002; Zhou and Wenger, 2013a,b) the initial OH

185   radical concentrations using H_2O_2 and HONO as precursor were (unit: molecule cm^{-3}): $(3.47$

186   $\pm 0.32) \times 10^6$ and $(8.34 \pm 1.36) \times 10^6$ respectively.

187

188   3. Results and discussion

189   3.1 Acenaphthylene photooxidation

190   The PTR-TOF-MS measurements performed in acenaphthylene photooxidation experiments

191   carried out under low and high-NO$_x$ conditions revealed 6 product peaks with m/z values

192   reported in Table S2. The temporal profiles of the identified ions are proposed in Figure 1.

193   Most of the reaction products are similar to those previously reported or for reactions

194   performed in the same chamber but using Cl atoms or O_3 to initiate oxidation (Reisen and

195   Arey, 2002; Zhou and Wenger, 2013b; Riva et al., 2015a; Riva et al., 2016). Based on

196   existing knowledge of the gas-phase chemistry of acenaphthylene, the peak at m/z 185 is

197   assigned to the protonated molecular ion $(M + H)^+$ of naphthalene-1,8-dicarbaldehyde

198   $(C_{12}H_8O_2)$ and a dialdehyde formed from OH addition to the aromatic rings. Previous studies

199   have reported large yields of both compounds from the photooxidation of acenaphthylene in

200   the presence of NO$_x$. The protonated ion at m/z 185 may have, however, more than 2 isomers.

201   Indeed, as discussed below and proposed in Scheme 1, formation of a protonated ion at m/z

202   183 $(C_{12}H_6O_2)$ and tentatively assigned as acenaphthenequinone cannot be explained by

203   solely the gas-phase oxidation of acenaphthenone $(C_{12}H_8O)$. Indeed, the abundance of

204   protonated ion at m/z 169 is likely too weak to explain the large signal observed for

205   acenaphthenequinone in the particulate phase (Figure 1). Therefore, formation of $C_{12}H_6O_2$

206 might also proceed through the gas-phase oxidation of hydroxy-acenaphthenone as tentatively

207 proposed in Scheme 1. Signals for the protonated ions at *m/z* 169 and 185 decrease

208 significantly after ca. 4000 s reaction time (Figure 1), suggesting that both primary reaction

209 products undergo further gas-phase oxidation and/or photolysis leading to secondary

210 generation compounds (Scheme 1). For instance, naphthalene-1,8-dicarbaldehyde may react

211 further with OH radicals or be photodissociated as observed for other aromatic aldehydes

212 (Wang et al., 2006).

213

214 Although the different compounds identified for each set of experiments were identical

215 under high- or low-NO_x conditions, their abundances were very different. As presented in

216 Figure 1, the abundances of ring-opening products (e.g. oxaacenaphthylene-2-one, 1,8-

217 naphthalic anhydride and 1,8-naphthalaldehydic acid) differ depending on the OH radical

218 precursor. Moreover, the high signals of small fragment ions detected by the ATOFMS

219 (Figure 2) at *m/z* 39 $(C_3H_3)^+$, 51 $(C_4H_3)^+$, 63 $(C_5H_3)^+$, 75 $(C_6H_3)^+$, 77 $(C_6H_5)^+$ and 115 $(C_9H_7)^+$

220 highlight the presence of ring-opening products in the particulate phase, as demonstrated in

221 previous studies using an ATOFMS at low laser energy (Riva et al., 2015a; Gross et al., 2000;

222 2005). The higher yield of ring opening products such as oxaacenaphthylene-2-one, 1,8-

223 naphthalic anhydride and 1,8-naphthalaldehydic acid in the gas phase (Figure 1) is consistent

224 with the higher signals for small fragment ions in the ATOFMS spectra (Figure 2), suggesting

225 that formation of ring-opening products is likely enhanced under low-NO_x conditions. This

226 observation is in contrast with experiments performed in the presence of NO_x. In that case,

227 ring-retaining species are enhanced, as revealed by the relatively larger abundances of

228 acenaphthenone (or its enol-form) and acenaphthenequinone (Figures 1 and 2) in both phases,

229 during the oxidation of acenaphthylene in the presence of HONO. It is worth noting that no

230 nitro compounds were identified in either gas or particle phases. Previous studies have,

231 however, reported the formation of nitro-products during the photooxidation of

232 acenaphthylene, but with very low yields, which likely explains the absence of nitro-products

233 in the mass spectra collected in this work (Arey et al., 1989; Reisen and Arey, 2002; Zhou and

234 Wenger, 2013b).

235

236 An extended reaction mechanism for the gas-phase oxidation of acenaphthylene is

237 proposed in Scheme 1. It is based on the PTR-TOF-MS data obtained in this work and also

238 builds on the results from previous experimental studies (Reisen and Arey, 2002; Zhou and

239 Wenger, 2013b). Oxidation of acenaphthylene is energetically favored at the unsaturated

240 cyclopenta-fused ring as highlighted in previous experimental (Atkinson and Aschmann,
241 1988; Reisen and Arey, 2002; Zhou and Wenger, 2013b; Riva et al., 2015a; Riva et al., 2016)
242 and theoretical studies (Dang et al., 2015). This double bond exhibits high reactivity and
243 explains the higher reactivity of acenaphthylene with atmospheric oxidants relative to other
244 PAHs. Hence acenaphthylene photooxidation is governed by the OH addition at the
245 unsaturated cyclopenta-fused ring. Due to the absence in our experiments of any nitro
246 compounds and the very small yields reported in previous work, the OH-adduct is expected to
247 mainly react with O_2. OH-acenaphthylene adduct could then lead to a peroxy radical (RO_2)
248 ($C_{12}H_9O_3^•$) and to acenaphthenone (and/or its enol-form). It has been reported that for simple
249 aldehydes and ketones, the keto form is the most stable and thus the equilibrium is likely
250 directed to the acenaphthenone (March, 1985). $C_{12}H_9O_3^•$ could then react with NO or go
251 through its self- /cross-reactions leading to the alkoxy radical ($C_{12}H_9O_2^•$). Two different
252 pathways are proposed for the fate of $C_{12}H_9O_2^•$, which appear to be as expected NO_x
253 dependent. Firstly, the ring-retaining channel could produce hydroxy-acenaphthenone, which
254 could further react and lead to acenaphthenequinone (Scheme 1). As discussed above, this
255 pathway appears to be likely favored in the presence of NO_x due to the relatively lower
256 abundance of small fragment ions in the mass spectrum of the ATOFMS as well as the larger
257 presence of ring-retaining products in both gas and particulate phases (Figures 1 and 2).
258 Secondly, $C_{12}H_9O_2^•$ can proceed through the ring-opening pathway occurring by C_1-C_2 bond
259 cleavage. As shown in Scheme 1, this reaction pathway leads exclusively to ring-opening
260 products, which appear to be favored under low-NO_x conditions. Naphthalene-1,8-
261 dicarbaldehyde and 1,8-naphthalaldehydic acid ($C_{12}H_8O_3$) are the two main primary products
262 arising from this ring-opening pathway and further react as shown in Figure 2 and proposed in
263 Scheme 1. As discussed above and reported in previous works (Zhou and Wenger, 2013b;
264 Riva et al., 2015a,b), naphthalene-1,8-dicarbaldehyde can yield 1,8-naphthalic anhydride from
265 H-atom abstraction of the aldehydic function, which would result in the formation of an RO_2
266 radical ($C_{12}H_7O_4^•$). Similarly to phthaldialdehyde, naphthalene-1,8-dicarbaldehyde could
267 undergo photodissociation, leading to 1,8-naphthalic anhydride (Wang et al., 2006; Riva et
268 al., 2015b). $C_{12}H_7O_4^•$ could then react with NO or RO_2 and form an acyl-oxy radical
269 ($C_{12}H_7O_3^•$). The chemistry of the resulting $C_{12}H_7O_3^•$ radical could proceed through the
270 bicyclic peroxy radical route in a fashion analogous to that proposed in Scheme 1. $C_{12}H_7O_3^•$
271 radical could also decarboxylate quickly (Chacon-Madrid et al., 2013) and the resulting
272 radical would react with O_2 leading to the formation of another RO_2 radical ($C_{11}H_7O_3^•$). As

9

273 presented in Scheme 1 and previously proposed, $C_{11}H_7O_3$•□could undergo cyclization and

274 lead to the formation of oxaacenaphthylene-2-one (Zhou and Wenger, 2013b).

275

276 It is important to point out that O_3 formation (~ 20 ppb final concentration) was

277 observed during the experiments carried out with HONO from the photolysis of NO_2. Due to

278 the high reactivity of acenaphthylene with ozone ((acenaphthylene + O_3); k = 3.99×10^{-16} cm^3

279 molecule^{-1} s^{-1}), O_3 might have participated in the formation of oxygenated species and

280 acenaphthylene depletion (Zhou and Wenger, 2013b). Due to the large UV- absorption band

281 overlap of acenaphthylene with ozone at wavelengths between 240 and 260 nm (Zander,

282 1969) it was not possible to determine an accurate contribution of ozone in the oxidation of

283 acenaphthylene. Riva et al. (2016) recently reported that a secondary ozonide ($C_{12}H_8O_3$) is the

284 main gas phase product arising from ozonolysis of acenaphthylene. In the high-NO_x

285 experiments, the product ion corresponding to $C_{12}H_8O_3$ was observed in very low abundances

286 (i.e. < 70 counts) indicating that the contribution of ozonolysis can be considered to be

287 negligible in the photo-oxidation experiments performed in this work.

288

289 3.2 Acenaphthene photooxidation.

290 Ten oxidation products from the reaction of OH radicals with acenaphthene were identified by

291 PTR-TOF-MS and the temporal profiles for the most abundant peaks are presented in Figure

292 3. These product peaks at *m/z* 133, 161, 169 and 177 were tentatively assigned to protonated

293 molecular ions of indanone (C_9H_8O), indanone carbaldehyde ($C_{10}H_8O_2$), acenaphthenone

294 ($C_{12}H_8O$) and oxoindan-carboxylic acid ($C_{10}H_8O_3$), respectively. Among these 4 products,

295 indanone carbaldehyde and acenaphthenone have been previously observed from the OH-

296 initiated oxidation of acenaphthene under high-NO_x conditions (Reisen and Arey, 2002; Zhou

297 and Wenger, 2013a). For instance, Reisen and Arey (2002) reported significant formation of

298 indanone carbaldehyde and estimated yields at 14-37%. Four other protonated ions were

299 observed at *m/z* 171, 183, 185 and 199 but in weaker abundance and were tentatively

300 assigned, based on existing knowledge of the gas-phase chemistry of acenaphthene, to

301 acenaphthenol ($C_{12}H_{10}O$), acenaphthequinone ($C_{12}H_6O_2$), naphthalene-1,8-dicarbaldehyde

302 ($C_{12}H_8O_2$) and 1,8-naphthalic anhydride ($C_{12}H_6O_3$), respectively. Finally, weak signals at *m/z*

303 187 and 200 measured only in the experiments performed in the presence of NO_x were

304 tentatively assigned to a dialdehyde ($C_{12}H_{10}O_2$) and nitroacenaphthene ($C_{12}H_9NO_2$). Proposed

305 products, and the ions used for their identification, are reported in Table S3.

306

307   The different products determined in this work are similar to those identified in

308   previous studies or during other experiments on acenaphthene performed in the same

309   environmental chamber but using Cl atoms as radical precursors (Reisen and Arey, 2002;

310   Zhou and Wenger, 2013a; Riva et al., 2015a). As observed in the case of the photooxidation

311   of acenaphthylene, the abundances of the different products were highly dependent on the

312   NO_x concentrations. The temporal profiles of the main compounds identified in the gas phase

313   were very different as presented in Figure 3. For example, formation of indanone and

314   indanone carbaldehyde during acenaphthene photooxidation under high-NO_x conditions was

315   higher, while their abundances remained low in the absence of NO_x. Moreover, the protonated

316   signal for acenaphthenone, which appears to be the main oxidation product from the

317   photooxidation of acenaphthene under low-NO_x conditions, was significantly higher

318   compared to the experiments carried out in the presence of NO_x. These observations highlight

319   that oxidation pathways or branching ratios highly depend on the NO_x concentration. Contrary

320   to the acenaphthylene system, ATOFMS spectra for acenaphthene SOA (Figure 4) reveal high

321   abundances of small fragment ions under low- and high-NO_x conditions, suggesting a high

322   contribution of aromatic ring-opening products. Thus, abundances of fragment ions in

323   ATOFMS spectra cannot be used to distinguish reaction pathways. Several species have been

324   identified in both the gas and particulate phases, corroborating a significant formation of

325   aromatic ring-opening products (Reisen and Arey, 2002; Zhou and Wenger, 2013a).

326

327   A proposed extended reaction mechanism for the gas-phase oxidation of acenaphthene

328   is presented in Scheme 2. It is based on the PTR-TOF-MS data obtained in this work and also

329   builds on the results from previous experimental studies (Reisen and Arey, 2002; Zhou and

330   Wenger, 2013a). The reaction of OH radicals with acenaphthene can, in principle, proceed via

331   three possible pathways: OH addition to the aromatic rings, H-atom abstraction from the

332   aromatic ring and H-atom abstraction from the saturated cylcopenta-fused ring. However, H-

333   atom abstraction from the aromatic rings has been demonstrated to be negligible compared to

334   OH addition for the oxidation of aromatic compounds (Calvert et al., 2002). Formation of

335   aromatic ring-opened dicarbonyls, such as indanone carbaldehyde or dialdehyde, is proposed

336   as shown in Scheme 2 to occur through OH addition to the aromatic rings followed by the

337   reaction of the OH-acenaphthene adduct with O_2 and further ring cleavages (Reisen and Arey,

338   2002). In this work, indanone carbaldehyde was observed as the major compound arising

339   from this OH-addition pathway. It is important to mention that secondary chemistry has not

340   been discussed in previous work, however, as presented in Figure 3, primary products

11

341 undergo further oxidation and lead to secondary products, including indanone and oxoindan-

342 carboxylic acid (Scheme 2).

343

344   The initial H-atom abstraction by OH radicals is followed by addition of O_2 leading to

345 a RO_2 radical ($C_{12}H_9O_2{}^\bullet$). Subsequent reactions with NO or RO_2 radicals proceed via two

346 pathways; (i) the molecular channel, which results in equimolar amounts of acenaphthenone

347 and acenaphthenol, and (ii) the radical channel which produces an RO radical ($C_{12}H_9O^\bullet$).

348 $C_{12}H_9O^\bullet$ can then further react with O_2 and lead to acenaphthenone as the sole product. As

349 proposed in Scheme 2 an alternative pathway, i.e. C-C bond cleavage of the $C_{12}H_9O^\bullet$ radical

350 followed by further oxidation could lead to the formation of naphthalene-1,8-dicarbaldehyde.

351 As described previously in the case of acenaphthylene, naphthalene-1,8-dicarbaldehyde could

352 further react or be photolyzed and lead to 1,8-naphthalic anhydride from the H-atom

353 abstraction of the aldehydic function. It is important to note that previous studies did not

354 consider this channel and attributed the formation of acenaphthequinone, naphthalene-1,8-

355 dicarbaldehyde and 1,8-naphthalic anhydride to analytical artifacts or from reactions with

356 acenaphthene impurities (Reisen and Arey, 2002; Sauret-Szczepanski and Lane, 2004).

357 Recently, Zhou and Wenger (2013a) investigated these potential analytical artifacts and

358 demonstrated the formation of naphthalene-1,8-dicarbaldehyde during acenaphthene

359 photooxidation. Acenaphthenone, acenaphthenequinone and 1,8-naphthalic anhydride were

360 also previously identified, ruling out the formation of these compounds as analytical artifacts.

361 Moreover, the abundances of these products observed in this work cannot be explained by

362 reactions of OH radicals or ozone with small amounts of acenaphthene impurities (e.g.

363 acenaphthylene, < 1%). Hence, our results complement those obtained by Zhou and Wenger

364 (2013a) highlighting the competition between OH addition to the aromatic rings and H-atom

365 abstraction from the cyclopenta-fused ring.

366

367   The competition between these two pathways appears to be different depending on the

368 NO_x concentration. As shown above, the relative abundances of the gas phase products were

369 very different in the presence and absence of NO_x (Figure 3). In the absence of NO_x, the

370 products from the OH-addition pathways (i.e. indanone, indanone carbaldehyde and

371 oxoindan-carboxylic acid) were observed in much lower abundances, suggesting that NO_x

372 could contribute to the stability of the OH-acenaphthene adduct (Nishino et al., 2012).

373 Conversely, products (i.e. acenaphthenone) from H-atom abstraction from the cyclopenta-

374 fused ring pathway were observed in relatively higher abundance in both gas- and particulate

12

375   phases. Although, the (acenaphthene + OH) reaction proceeds through two different pathways

376   under low-NO_x conditions, it is difficult to distinguish which one dominates the global

377   mechanism presented in Scheme 2. Previous studies have evaluated the competition between

378   OH addition to the aromatic ring and H-atom abstraction (from aromatic rings) pathways:

379   under atmospheric conditions the mechanism of reaction of OH radicals with aromatic

380   hydrocarbons occurs mainly (i.e. > 90%) via addition to the aromatic ring (Calvert et al.,

381   2002; Atkinson and Arey, 2007). Therefore, the results presented in this work suggest that the

382   competition between OH-addition and H-atom abstraction from the cyclopenta-fused ring is

383   more important than previously expected. Hence, the OH oxidation of acenaphthene could

384   also be governed by H-atom abstraction from the cyclopenta-fused ring depending on the

385   concentration of NO_x. More work is, however, needed to quantify the branching ratio between

386   both pathways.

387

388   3.3 SOA formation.

389   Rapid SOA formation was observed in all experiments immediately after the formation of OH

390   radicals. Using a semi-empirical model for SOA formation based on the gas-particle

391   partitioning equilibrium of semi volatile products (Odum et al., 1996), the SOA yields (Y),

392   were determined from the experiments performed under low- /high-NO_x conditions to be

393   0.61/0.46 and 0.68/0.55 for acenaphthylene and acenaphthene, respectively (Table 1). The

394   volume concentration was corrected for particle wall loss by applying size-dependent first-

395   order loss coefficients after SOA growth was finished. The indicated uncertainties (2σ) in

396   Table 1 correspond to scatter in particle volume measurements. The aerosol mass was

397   calculated using volume concentrations measured by SMPS and assuming a particle density

398   of 1.4 g cm^{-3} (Chan et al., 2009; Shakya and Griffin, 2010). The high concentrations used in

399   this work probably enhanced partitioning of semi volatile species to the particle phase

400   resulting in SOA yields that are larger than might be expected under more realistic

401   atmospheric conditions. Nevertheless, the high yields determined in this work further

402   illustrate the important potential of PAHs to form SOA from their oxidation by OH radicals.

403   The first study reporting SOA formation yields from the photooxidation of acenaphthene and

404   acenaphthylene under high- and low-NO_x conditions was proposed by Shakya and Griffin

405   (2010). The SOA yields proposed in the previous work (0.04-0.13 and 0.03-0.11 for

406   acenaphthylene and acenaphthene photooxidation respectively) are much lower than those

407   reported here. It is worth noting that, even though similar initial PAH concentrations were

408   used, large discrepancies exist between the SOA yields reported by Chan et al. (2009) and

13

409 Shakya and Griffin (2010) for naphthalene photooxidation. Indeed, Shakya and Griffin (2010)

410 proposed yields in the range of 0.08-0.16, while Chan et al. (2009) determined yields to be

411 0.19-0.74. As discussed by Chen et al. (2016), differences of SOA yields could be attributed

412 to different chamber conditions such as light intensity, NO_x levels, OH radicals, and organic

413 mass loading. In the case of aromatic chemistry, it has been shown that photolysis processes

414 play a major role in the loss of carbonyl products (Wang et al., 2006; Clifford et al., 2011).

415 For instance, aromatic aldehydes can be photodissociated, leading to the formation of more

416 oxidized compounds, which could further contribute to SOA formation (Wang et al., 2006).

417 Furthermore, Warren et al. (2010) have reported the importance of light intensity in SOA

418 formation from the photooxidation of monoaromatics. Therefore, in addition to the high

419 concentration of PAHs, higher photolysis rates could also explain the subsequent SOA yields

420 determined in this work.

421

422 Under high-NO_x conditions, the photolysis of HONO generated relatively high

423 concentrations of OH (i.e. 8.4×10^6 molecule cm^{-3}), leading to rapid acenaphthene and

424 acenaphthylene consumption. Under low-NO_x conditions, aerosol growth was also observed

425 immediately after the lights were turned on. Nevertheless, the PAH consumption appeared to

426 be slower than under high-NO_x conditions, owing to the relatively low concentration of OH

427 radicals produced by H_2O_2 photolysis. Figure S1 presents the time-dependent growth curves

428 (i.e. the mass of organic aerosol generated, noted as ΔMo, as a function of reacted PAH, ΔHC)

429 for acenaphthene and acenaphthylene reactions with OH radicals under high- and low-NO_x

430 conditions. For all experiments, a constant increase of aerosol mass was observed and reached

431 its maximum when acenaphthylene or acenaphthene was totally consumed. No clear

432 difference was found between the high- and low-NO_x conditions, indicating that compounds

433 produced during the photooxidation of PAHs likely participate in SOA growth. Similar trends

434 have been observed previously during the photooxidation of biogenic and anthropogenic

435 precursors (Ng et al., 2006; Chan et al., 2009). The fact that aerosol growth stopped when the

436 precursor was consumed indicates that the first oxidation reaction is the rate-determining step

437 in SOA formation. In this case, the primary products could directly condense and participate

438 in SOA formation, and therefore contribute to aerosol growth.

439

440 4. Conclusion

441 In this work, both gas and particle phase products from the OH oxidation of acenaphthylene

442 and acenaphthene were characterized using two on-line techniques (i.e. PTR-TOF-MS and

14

443   ATOFMS). The impact of NO_x on product distributions and SOA formation was explored for

444   these compounds for the first time. Based on these results, extended mechanisms for the gas-

445   phase oxidation of acenaphthylene and acenaphthene are proposed suggesting additional

446   pathways and previously unidentified compounds under the conditions used in this work. The

447   OH oxidation of acenaphthylene under high- and low-NO_x conditions is mainly governed by

448   OH addition. The significant production of products such as acenaphthenequinone or 1,8-

449   naphthalic anhydride suggests preferential OH addition to the unsaturated cyclopenta-fused

450   ring. On the contrary, acenaphthene oxidation begins with OH radical addition to the aromatic

451   ring followed by the reaction of the resultant OH-adduct with O_2 and further ring cleavages in

452   the presence of NO_x. H-atom abstraction from the saturated cyclopenta-fused ring appears,

453   however, not to be negligible as stipulated in previous work, especially in the absence of NO_x.

454   Indeed, products from the H-atom abstraction pathway, such as acenaphthenone, exhibit a

455   higher importance in the experiments performed in absence of NO_x. In addition, secondary

456   chemistry was identified in all experiments and is now proposed in the extended mechanisms.

457   The oxidation of acenaphthene and acenaphthylene formed SOA in large yields and suggest

458   that the reaction of OH radicals with PAHs could contribute to anthropogenic SOA formation.

459   It is shown that SOA growth is relatively linear and completes when the precursor

460   hydrocarbon is consumed. Such observations illustrate that SOA formation is mainly due to

461   the first generation products proceeding through gas-to-particle conversion processes. SOA

462   formation yields are higher under low-NO_x conditions than under high-NO_x conditions as

463   previously reported for the photooxidation of other aromatic compounds. Further

464   experimental works on SOA formation from the photooxidation of acenaphthylene and

465   acenaphthene is, however needed to better evaluate the impact of light intensity and NO_x

466   mixing ratio on the different oxidation pathways.

467

468

15

469　AUTHOR INFORMATION

470　Corresponding authors:

471　John C. Wenger

472　　　　Email: j.wenger@ucc.ie

473　　　　Phone: +353 21 490 3000

474　Eric Villenave

475　　　　Email: e.villenave@epoc.u-bordeaux1.fr

476　　　　Phone: +33 5 4000 6350

477

16

References

Arey, J.; Zielinska, B.; Atkinson, R.; Aschmann, S.M. Nitroarene products from the gas-phase reactions of volatile polycyclic aromatic hydrocarbons with the OH radical and N_2O_5. *Int. J. Chem. Kinet.* **1989**, 21, 775–799.

Atkinson, R.; Aschmann, S.M. Kinetics of the gas phase reactions of acenaphthene and acenaphthylene and structurally-related aromatic compounds with OH and NO_3 radicals, N_2O_5 and O_3 at 296 ± 2 K. *Int. J. Chem. Kinet.* **1988**, 20, 513–539.

Atkinson, R.; Arey, J. Atmospheric chemistry of gas-phase polycyclic aromatic hydrocarbons: Formation of atmospheric mutagens. *Environ. Health Presp.* **1994**, 102, 117–126.

Atkinson, R.; Arey, J. Mechanisms of the gas-phase reactions of aromatic hydrocarbons and PAHs with OH and NO_3 radicals. *Polycycl. Aromat. Comp.* **2007**, 27, 15–40.

Banceau, C.E.; Mihele, C.; Lane, D.A.; Bunce, N.J. Reactions of methylated naphthalenes with hydroxyl radicals under simulated atmospheric conditions. *Polycycl. Aromat. Comp.* **2001**, 18, 415–425.

Brubaker Jr., W.W.; Hites, R.A. OH reaction kinetics of polycyclic aromatic hydrocarbons and polychlorinated dibenzo-p-dioxins and dibenzofurans. *J. Phys. Chem. A* **1998**, 102, 915–921.

Calvert, J.G.; Atkinson, R.; Becker, K.H.; Kamens, R.M.; Seinfeld, J.H.; Wallington, T.J.; Yarwood, G. The mechanisms of atmospheric oxidation of aromatic hydrocarbons. *Oxford university press*, 2002, pp. 556.

Cappelin, L.; Karl, T.; Probst, M.; Ismailova, O.; Winkler, P.M.; Soukoulis, C.; Aprea, E.; Märk, T.D.; Gasperi, F.; Biasioli, F. On quantitative determination of volatile organic compound concentration using proton transfer reaction time-of-flight mass spectrometry. *Environ. Sci. Technol.* **2012**, 46, 2283–2290.

Chacon-Madrid, H.J.; Henry, K.M.; Donahue, N.M. Photo-oxidation of pinonaldehyde at low NO_x: from chemistry to organic aerosol formation. *Atmos. Chem. Phys.* **2013**, 13, 3227–3236.

Chan, A.W.H.; Kautzman, K.E.; Chhabra, P.S.; Surratt, J.D.; Chan, M.N.; Crounse, J.D.; Kürten, A.; Wennberg, P.O.; Flagan, R.C.; Seinfeld, J.H. Secondary organic aerosol formation from

519 photooxidation of naphthalene and alkylnaphthalenes: implications for oxidation of intermediate
520 volatility organic compounds (IVOCs). *Atmos. Chem. Phys.* **2009**, 9, 3049–3060.

521

522 Chang, K.-F.; Fang, G.-C.; Chen, J.-C.; Wu, Y.-S. Atmospheric polycyclic aromatic hydrocarbons
523 (PAHs) in Asia: a review from 1999 to 2004. *Environ. Pollut.* **2006**, 142, 388–396.

524

525 Chen, C.-L.; Kacarab, M.; Tang, P.; Cocker III, D.R. SOA formation from naphthalene, 1-
526 methylnaphthalene, and 2-methylnaphthalene photooxidation. *Atmos. Environ.* **2016**, 131, 424–
527 453.

528

529 Clifford, G.M.; Hadj-Aïssa, A.; Healy, R.M.; Mellouki, A.; Muñoz, A.; Wirtz, K.; Martín Reviejo,
530 M.; Borrás, E.; Wenger, J.C. The atmospheric photolysis of o-tolualdehyde. *Environ. Sci. Technol.*
531 **2011**, 40, 9649–9657.

532

533 Cox, R.A. The photolysis of nitrous acid in the presence of carbon monoxide and sulphur dioxide.
534 *J. Photochem.* **1974**, 3, 291–304.

535

536 Dang, J.; Shi, X.; Zhang, Q.; Hu, J.; Wang, W. Mechanism and thermal rate constant for the gas-
537 phase ozonolysis of acenaphthylene in the atmosphere. *Sci. Tot. Environ.* **2015**, 514, 344–350.

538

539 Dejean, S.; Raynaud, C.; Meybeck, M.; Della Massa, J.-P.; Simon, V. Polycyclic aromatic
540 hydrocarbons (PAHs) in atmospheric urban area: monitoring on various types of sites. *Environ.*
541 *Monit. Assess.* **2009**, 148, 27–37.

542

543 Ervens, B.; Turpin, B.J.; Weber, R.J. Secondary organic aerosol formation in cloud droplets and
544 aqueous particles (aqSOA): A review of laboratory, field and model studies. *Atmos. Chem. Phys.*
545 **2011**, 11, 11069–11102.

546

547 Estève, W.; Budzinski, H.; Villenave, E. Heterogeneous reactivity of OH radicals with
548 phenanthrene. *Polycycl. Aromat. Comp.* **2003**, 23, 441-456.

549

550 Galloway, M.M.; Chhabra, P.S.; Chan, A.W.H.; Surratt, J.D.; Flagan, R.C.; Seinfeld, J.H.;
551 Keutsch, F.N. Glyoxal uptake on ammonium sulphate seed aerosol: reaction products and
552 reversibility of uptake under dark and irradiated conditions. *Atmos. Chem. Phys.* **2009**, 9, 3331–
553 3345.

554

555 Gard, E.; Mayer, J.E.; Morrical, B.D.; Dienes, T.; Fergenson, D.P.; Prather, K.A. Real-time
556 analysis of individual atmospheric aerosol particles: Design and performance of a portable
557 ATOFMS. *Anal. Chem.* **1997**, 69, 4083–4091.

559 Gross, D.S.; Galli, M.E.; Silva, P.J.; Wood, S.H.; Liu, D.-Y.; Prather, K.A. Single particle
560 characterization of automobile and diesel truck emissions in the Caldecott Tunnel. *Aerosol Sci.*
561 *Technol.* **2000**, 32, 152–163.

563 Gross, D. S.; Barron, A. R.; Sukovich, E. M.; Warren, B. S.; Jarvis, J. C.; Suess, D. T.; Prather, K.
564 A. Stability of single particle tracers for differentiating between heavy- and light-duty vehicle
565 emissions. *Atmos. Environ.* **2005**, 39, 2889–2901.

567 Hallquist, M.; Wenger, J.C.; Baltensperger, U.; Rudich, Y.; Simpson, D.; Claeys, M.; Dommen, J.;
568 Donahue, N.M.; George, C.; Goldstein, A.H.; Hamilton, J.F.; Herrmann, H.; Hoffmann, T.;
569 Iinuma, Y.; Jang, M.; Jenkin, M.E.; Jimenez, J.L.; Kiendler-Scharr, A.; Maenhaut, W.;
570 McFiggans, G.; Mentel, Th.F.; Monod, A.; Prévôt, A.S.H.; Seinfeld, J.H.; Surratt, J.D.;
571 Szmigielski, R.; Wildt, J. The formation, properties and impact of secondary organic aerosol:
572 current and emerging issues. *Atmos. Chem. Phys.* **2009**, 9, 5155–5236.

574 Hanedar, A.; Alp, K.; Kaynak, B.; Avsar, E. Toxicity evaluation and source apportionment of
575 polycyclic aromatic hydrocarbons (PAHs) at three stations in Istanbul, Turkey. *Sci. Tot. Environ.*
576 **2014**, 488, 437–446.

578 Healy, R.M.; Chen, Y.; Kourtchev, I.; Kalberer, M.; O'Shea, D.; Wenger, J.C. Rapid formation of
579 secondary organic aerosol from the photolysis of 1-nitronaphthalene: role of naphthoxy radical
580 self-reaction. *Environ. Sci. Technol.* **2012**, 46, 11813–11820.

582 Ho, K.F.; Ho, S.S.H.; Lee, S.C.; Cheng, Y.; Chow, J.C.; Watson, J.G.; Louie, P.K.K.; Tian, L.W.
583 Emissions of gas- and particle-phase polycyclic aromatic hydrocarbons (PAHs) in the Shing Mun
584 Tunnel, Hong Kong. *Atmos. Environ.* **2009**, 43, 6343–6351.

586 Kautzman, K.E.; Surratt, J.D.; Chan, M.N.; Chan, A.W.H.; Hersey, S.P.; Chhabra, P.S.; Dalleska,
587 N.F.; Wennberg, P.O.; Flagan, R.C.; Seinfeld, J.H. Chemical composition of gas- and aerosol-
588 phase products from the photooxidation of naphthalene. *J. Phys. Chem. A* **2010**, 114, 913–934.

590 Keyte, I.J.; Harrison, R.M.; Lammel, G. Chemical reactivity and long-range transport potential of
591 polycyclic aromatic hydrocarbons – a review. *Chem. Soc. Rev.* **2013**, 42, 9333–9391.

592

593   Kleindienst, T.E.; Jaoui, M.; Lewandowski, M.; Offenberg, J.H.; Docherty, K.S. The formation of
594   SOA and chemical tracer compounds from the photooxidation of naphthalene and its methyl
595   analogs in the presence and absence of nitrogen oxide. *Atmos. Chem. Phys.* **2012**, 12, 8711–8726.

596   Kourtchev, I.; Bejan, I.; Sodeau, J.R.; Wenger, J.C. Gas-phase reaction of (E)-β-farnesene with
597   ozone: Rate coefficient and carbonyl products. *Atmos. Environ.* **2009**, 43, 3182–3190.

598

599   Kroll, J.H.; Seinfeld, J.H. Chemistry of secondary organic aerosol: formation and evolution of
600   low-volatility organics in the atmosphere. *Atmos. Environ.* **2008**, 42, 3593–3624.

601

602   Lee, J.Y.; Lane, D.A. Unique products from the reaction of naphthalene with the hydroxyl radical.
603   *Atmos. Environ.* **2009**, 43, 4886–4893.

604

605   Lin, P.-H.; Pan, W.-C.; Kang, Y.-W.; Chen, Y.-L.; Lin, C.-H.; Lee, M.-C.; Chou, Y.-H.;
606   Nakamura, J. Effects of naphthalene quinonoids on the induction of oxidative DNA damage and
607   cytotoxicity in calf thymus DNA and in human cultured cells. *Chem. Res. Toxicol.* **2005**, 18,
608   1262–1270.

609

610   Marais, E.A.; Jacob, D.J.; Jimenez, J.L.; Campuzano-Jost, P.; Day, D.A.; Hu, W.; Krechmer, J.;
611   Zhu, L.; Kim, P.S.; Miller, C.C.; Fisher, J.A.; Travis, K.; Yu, K.; Hanisco, T.F.; Wolfe, G.M.;
612   Arkinson, H.L.; Pye, H.O.T.; Froyd, K.D.; Liao, J.; McNeill, V.F. Aqueous-phase mechanism for
613   secondary organic aerosol formation from isoprene: application to the southeast United States and
614   co-benefit of SO_2 emission controls. *Atmos. Chem. Phys.* **2016**, 16, 1603–1618.

615

616   March, J. Advanced Organic Chemistry, 3rd ed.; *John Wiley & Sons*: New York, 1985; pp 66–68.

617

618   Ng, N.L.; Kroll, J.H.; Keywood, M.D.; Bahreini, R.; Varutbangkul, V.; Flagan, R.C.; Seinfeld,
619   J.H.; Lee, A.; Goldstein, A.H. Contribution of first- versus second-generation products to
620   secondary organic aerosols formed in the oxidation of biogenic hydrocarbons. *Environ. Sci.*
621   *Technol.* **2006**, 40, 2283–2297.

622

623   Nishino, N.; Arey, J.; Atkinson, R. 2-Formylcinnamaldehyde formation yield from the OH
624   radical-initiated reaction of naphthalene: effect of NO_2 concentration. *Environ. Sci. Technol.* **2012**,
625   46, 8198–8204.

626

627   Odum, J.R.; Hoffmann, T.; Bowman, F.; Collins, D.; Flagan, R.C.; Seinfeld, J. H. Gas/particle
628   partitioning and secondary organic aerosol yields. *Environ. Sci. Technol.* **1996**, 30, 2580–2585.

629

630 Pope III, C.A.; Dockery, D.W. Health effects of fine particulate air pollution: lines that connect. *J.*
631 *Air Waste Manage. Assoc.* **2006**, 56, 709–742.

632

633 Pye, H.O.T.; Pouliot, G.A. Modeling the role of alkanes, polycyclic aromatic hydrocarbons, and
634 their oligomers in secondary organic aerosol formation. *Environ. Sci. Technol.* **2012**, 46, 6041–
635 6047.

636

637 Pye, H.O.T.; Pinder, R.W.; Piletic, I.R.; Xie, Y.; Capps, S.L.; Lin, Y.-H.; Surratt, J.D.; Zhang, Z.;
638 Gold, A.; Luecken, D.J.; Hutzell, W.T.; Jaoui, M.; Offenberg, J.H.; Kleindienst, T.E.;
639 Lewandowski, M.; Edney, E.O. Epoxide pathways improve model predictions of isoprene markers
640 and reveal key role of acidity in aerosol formation. *Environ. Sci. Technol.* **2013**, 47, 11056–11064.

641

642 Reisen, F.; Arey, J. Reactions of hydroxyl radicals and ozone with acenaphthene and
643 acenaphthylene. *Environ. Sci. Technol.* **2002**, 36, 4302–4311.

644

645 Riva, M.; Healy, R.M.; Flaud, P-.M.; Perraudin, E.; Wenger, J.C.; Villenave, E. Kinetics of the
646 gas-phase reactions of chlorine atoms with naphthalene, acenaphthene and acenaphthylene. *J.*
647 *Phys. Chem. A* **2014**, 118, 3535–3540.

648

649 Riva, M.; Healy, R.M.; Flaud, P-.M.; Perraudin, E.; Wenger, J.C.; Villenave, E. Gas- and particle-
650 phase products from the chlorine-initiated oxidation of polycyclic aromatic hydrocarbons. *J. Phys.*
651 *Chem. A* **2015a**, 119, 11170–11181.

652

653 Riva, M.; Robinson, E.S.; Perraudin, E.; Donahue, N.M.; Villenave, E. Photochemical aging of
654 secondary organic aerosols generated from the photooxidation of polycyclic aromatic
655 hydrocarbons in the gas-phase. *Environ. Sci. Technol.* **2015b**, 49, 5407–5416.

656

657 Riva, M.; Tomaz, S.; Cui, T.; Lin, Y.-H.; Perraudin, E.; Gold, A.; Stone, E. A.; Villenave E.;
658 Surratt, J.D. Evidence for an unrecognized secondary anthropogenic source of organosulfates and
659 sulfonates: gas-phase oxidation of polycyclic aromatic hydrocarbons in the presence of sulfate
660 aerosol. *Environ. Sci. Technol.* **2015c**, 49, 6654–6664.

661

662 Riva, M.; Healy, R.M.; Tomaz, S.; Flaud, P-.M.; Perraudin, E.; Wenger, J.C.; Villenave, E. Gas-
663 and particulate phase products from the ozonolysis of acenaphthylene. *Atmos. Environ.*
664 **2016**, 142, 104–113.

665

666 Robinson, A.L.; Donahue, N.M.; Shrivastava, M.K.; Weitkamp, E.; Sage, A.M.; Grieshop, A. P.;
667 Lane, T.E.; Pierce, J.R.; Pandis, S.N. Rethinking organic aerosols: semivolatile emissions and
668 photochemical aging. *Science* **2007**, 315, 1259–1262.

669 Sasaki, J.; Aschmann, S.M.; Kwok, E.S.C.; Atkinson, R.; Arey, J. Products of the gas-phase OH
670 and NO_3 radical-initiated reactions of naphthalene. *Environ. Sci. Technol.* **1998**, 31, 3173–3179.

671

672 Sauret-Szczepanski, N.; Lane, D.A. Smog chamber study of acenaphthene: gas-particle partition
673 measurements of the products formed by reaction with the OH radical. *Polycycl. Aromat. Comp.*
674 **2004**, 24, 161–172.

675

676 Shakya, K.M.; Griffin, R.J. Secondary organic aerosol from photooxidation of polycyclic aromatic
677 hydrocarbons. *Environ. Sci. Technol.* **2010**, 44, 8134–8139.

678

679 Silva, P.J.; Prather, K.A. Interpretation of mass spectra from organic compounds in aerosol time-
680 of-flight mass spectrometry. *Anal. Chem.* **2000**, 72, 3553–3562.

681

682 Surratt, J.D.; Gomez-Gonzalez, Y.; Chan, A.W.H.; Vermeylen, R.; Shahgholi, M.; Kleindienst,
683 T.E.; Edney, E.O.; Offenberg, J.H.; Lewandowski, M.; Jaoui, M.; Maenhaut, W.; Claeys, M.;
684 Flagan, R.C.; Seinfeld, J.H. Organosulfate formation in biogenic secondary organic aerosol. *J.*
685 *Phys. Chem. A* **2008**, 112, 8345–8378.

686

687 Thüner, L.P.; Bardini, P.; Rea, G.J.; Wenger, J.C. Kinetics of the gas-phase reactions of OH and
688 NO_3 radicals with dimethylphenols. *J. Phys. Chem. A* **2004**, 108, 11019-11025.

689

690 Tkacik, D.S.; Presto, A.A.; Donahue, N.M.; Robinson, A.L. Secondary organic aerosol formation
691 from intermediate-volatility organic compounds: cyclic, linear, and branched alkanes. *Environ.*
692 *Sci. Technol.* **2012**, 46, 8773–8781.

693

694 Volkamer, R.; Jimenez, J.L.; San Martini, F.; Dzepina, K.; Zhang, Q.; Salcedo, D.; Molina, L.T.;
695 Worsnop, D.R.; Molina, M.J. Secondary organic aerosol formation from anthropogenic air
696 pollution: Rapid and higher than expected. *Geophys. Res. Lett.* **2006**, 33, L17811.

697

698 Wang, L.; Arey, J.; Atkinson, R. Kinetics and products of photolysis and reaction with OH
699 radicals of a series of aromatic carbonyl compounds. *Environ. Sci. Technol.* **2006**, 40, 5465–5471.

700

701   Warren, B.; Song, C.; Cocker, D.R. Light intensity and light source influence on secondary
702   organic aerosol formation for the *m*-xylene/NO$_x$ photooxidation system. *Environ. Sci. Technol.*
703   **2008**, 42, 5461–5466.

704

705   Zander, M. Notiz uber dimeres biacenaphthylenyl-(1.1') („Di-perinaphthylenbutadien"). *Chem.*
706   *Ber.* **1969**, 102, 3599–3602.

707

708   Zelenyuk, A.; Imre, D. Single particle laser ablation time-of-flight mass spectrometer: An
709   introduction to SPLAT. *Aerosol Sci. Tech.* **2005**, 39, 554–568.

710

711   Zhou, S.; Wenger, J.C. Kinetics and products of the gas-phase reactions of acenaphthene with
712   hydroxyl radicals, nitrate radicals and ozone. *Atmos. Environ.* **2013a**, 72, 97–104.

713

714   Zhou, S.; Wenger, J.C. Kinetics and products of the gas-phase reactions of acenaphthylene with
715   hydroxyl radicals, nitrate radicals and ozone. *Atmos. Environ.* **2013b**, 75, 103–112.

716

717   Zimmermann, R.; Ferge, T.; Galli, M.; Karlsson, R. Application of single-particle laser
718   desorption/ionization time-of-flight mass spectrometry for detection of polycyclic aromatic
719   hydrocarbons from soot particles originating from an industrial combustion process. *Rapid*
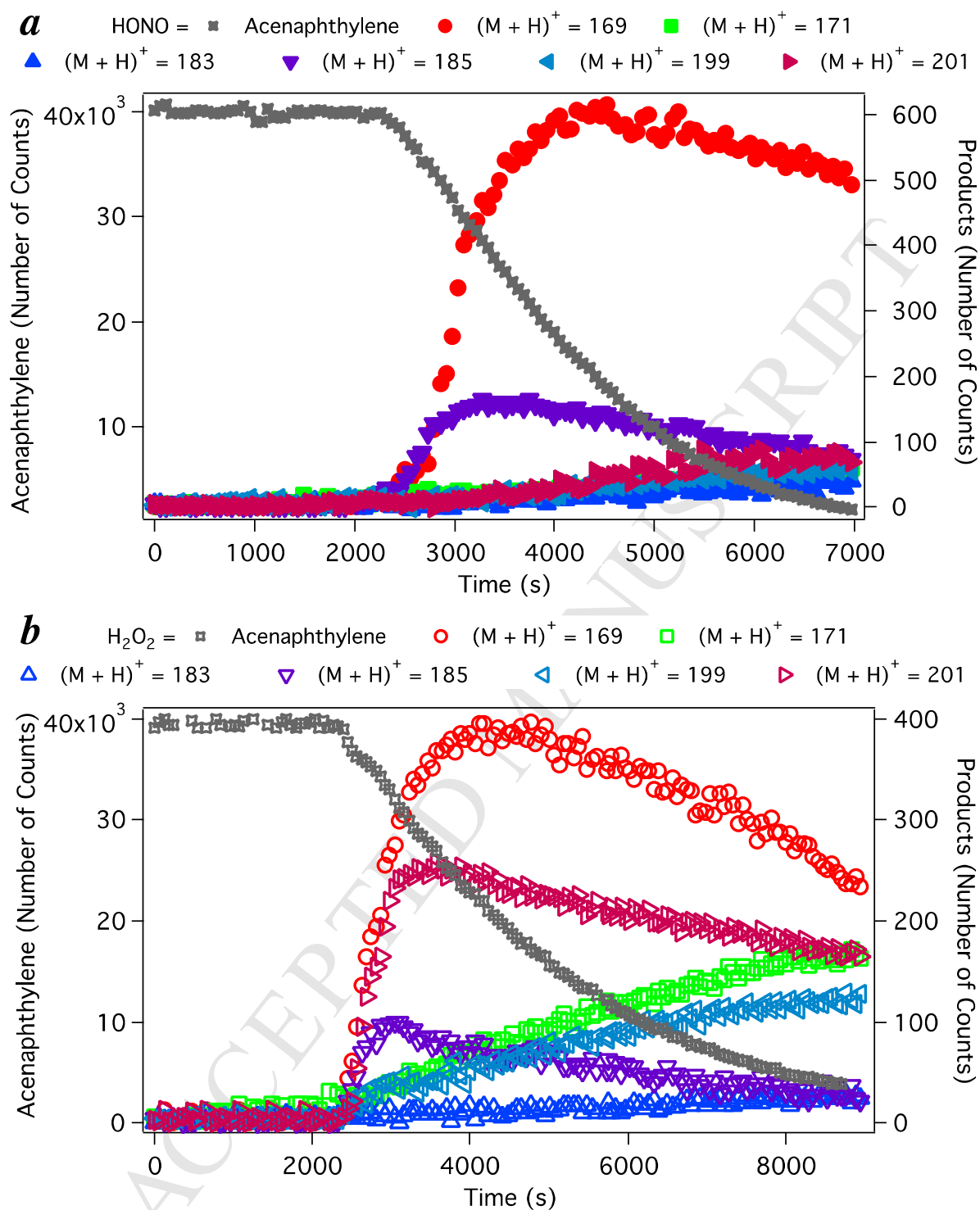720   *Commun. Mass Spectrom.* **2003**, 17, 851–859.

23

Figure 1. Temporal profiles of major ions identified by PTR-TOF-MS from the gas-phase oxidation of acenaphthylene initiated by OH radicals (full and open markers represent experiments performed under high- (*a*) and low-NO$_x$ (*b*) conditions, respectively).
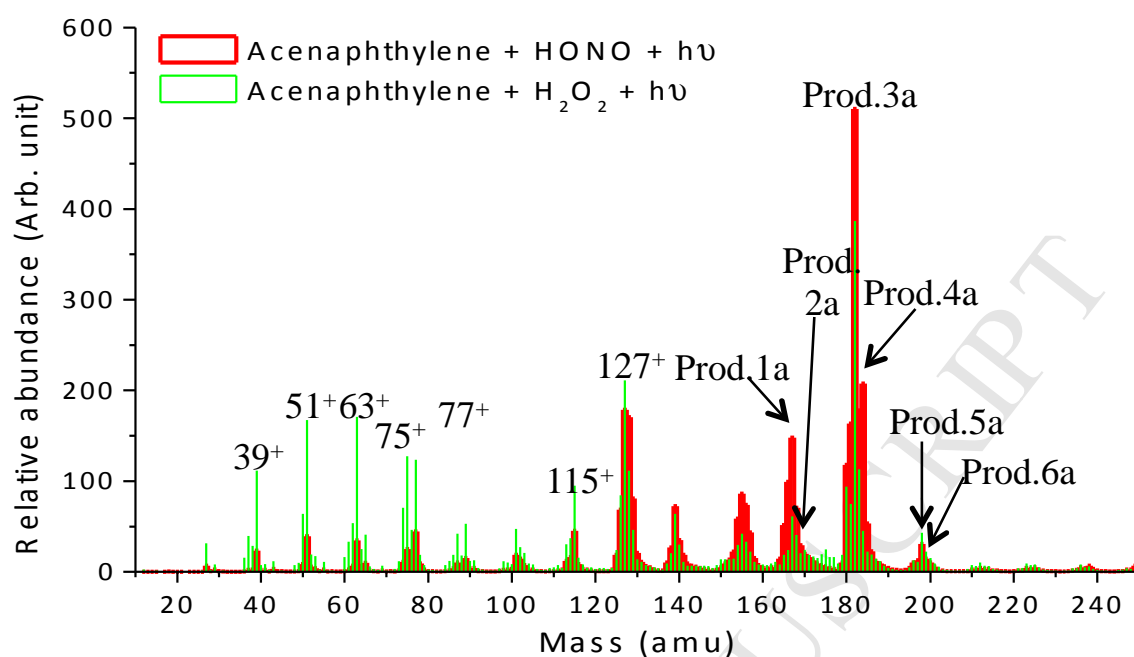
726

727 **Figure 2**. ATOFMS average mass spectra (positive ion mode) using a laser pulse of 0.2 mJ for SOA

728 formed from the photooxidation of acenaphthylene under high- (red) and low-NO_x (green) conditions.
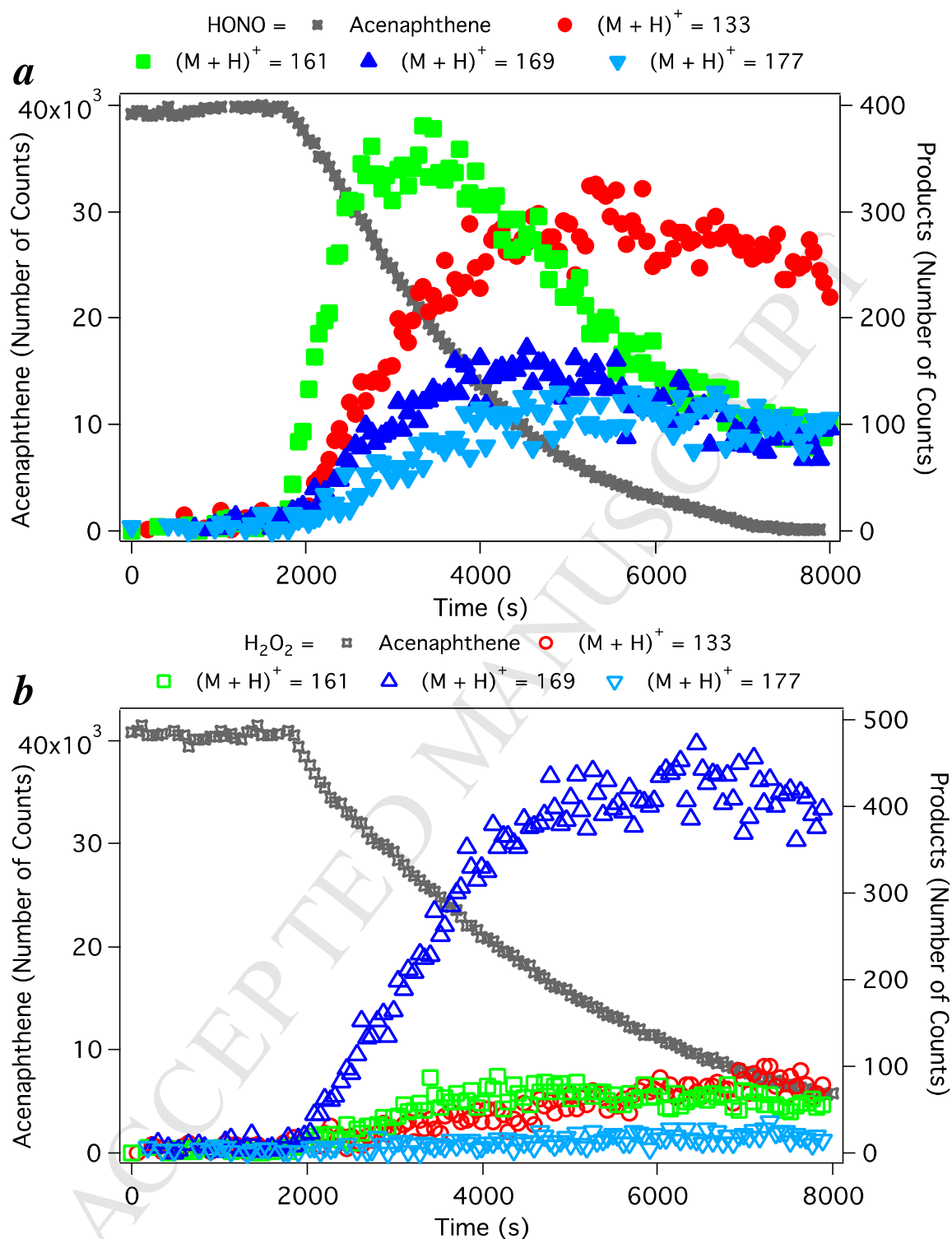
729

Figure 3. Main gas-phase compounds identified during the photooxidation of acenaphthene using PTR-TOF-MS (full and open markers represent experiments performed under high- (*a*) and low-NO$_x$ (*b*) conditions, respectively).
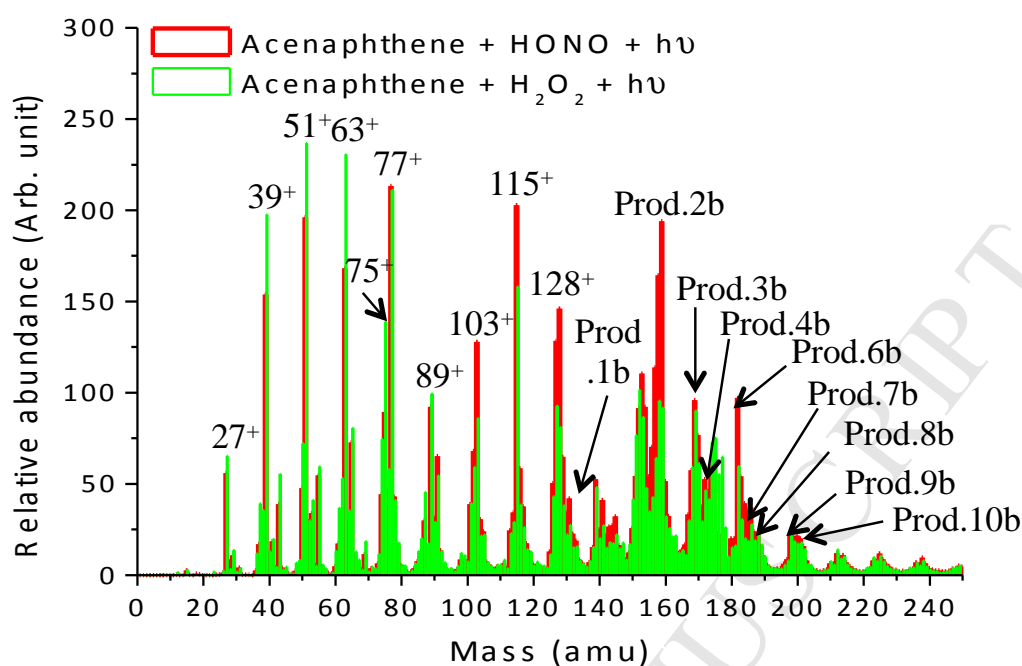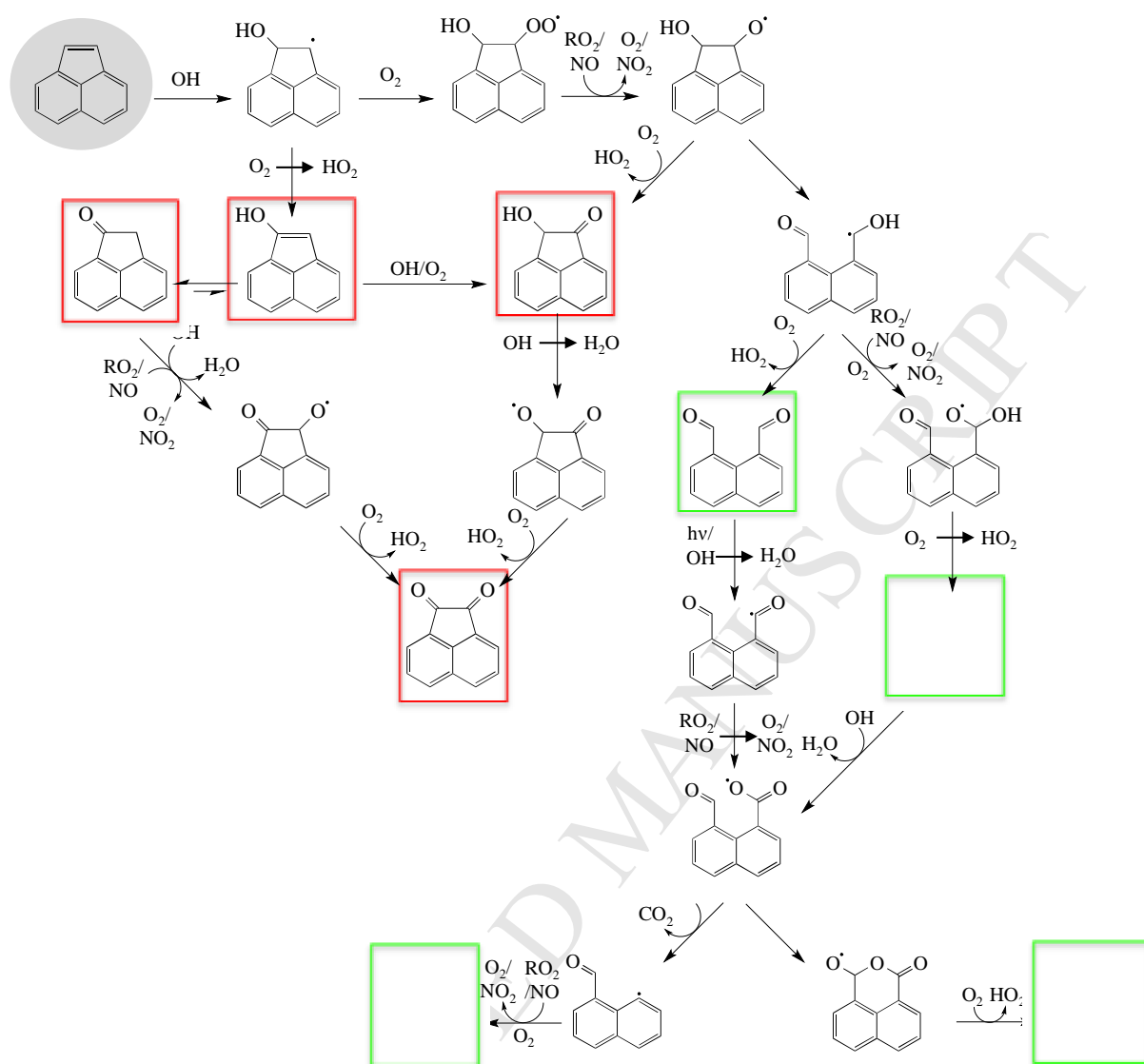
735

736 **Figure 4**. ATOFMS average mass spectra (positive ion mode) using a laser pulse of 0.2 mJ for SOA

737 formed from the photooxidation of acenaphthene under high- (red) and low-NO$_x$ (green) conditions.

738

739

740 **Scheme 1**. Proposed mechanism for the photooxidation of acenaphthylene (green and red boxes

741 represent the favored products formed under low- and high-NO_x conditions respectively).

742

743

744 **Scheme 2**. Proposed mechanism for the photooxidation of acenaphthene (green and red boxes

745 represent the favored products formed under low- and high-NO$_x$ conditions respectively).
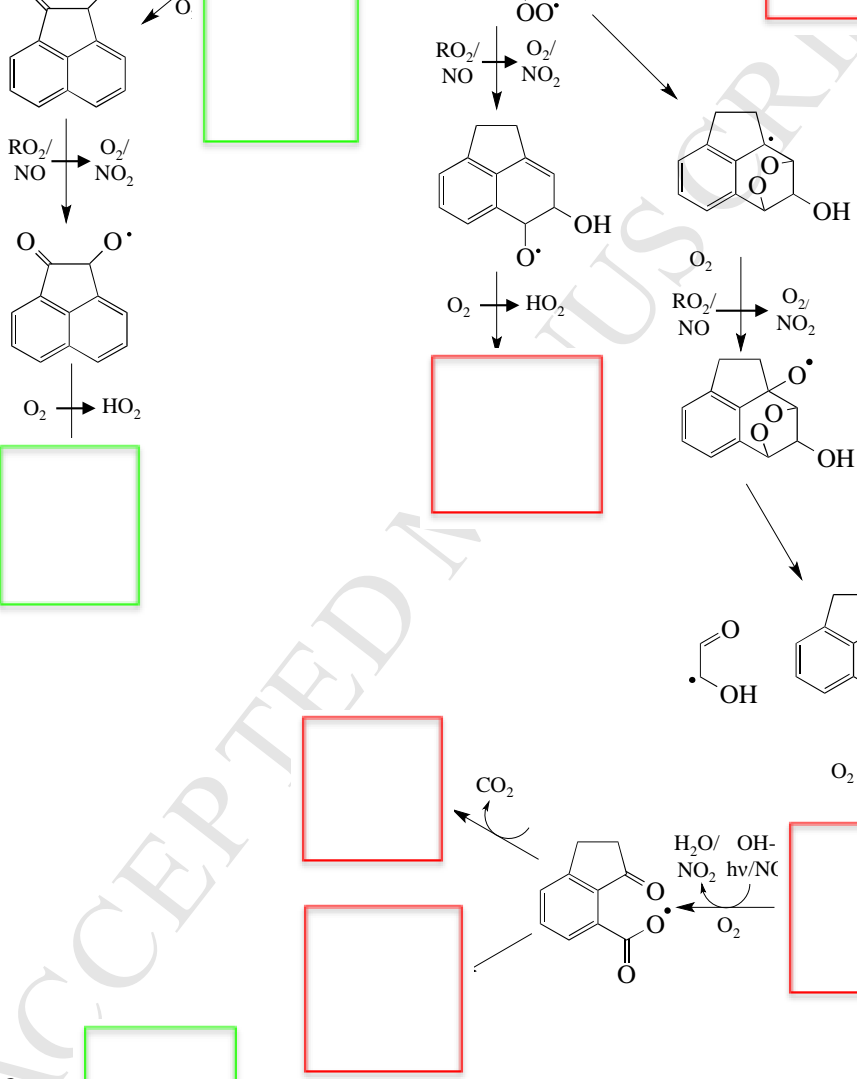
HIGHLIGHTS

Identification of competitive pathways for the OH-initiated oxidation of Acenaphthene

Formation of ring-opening products favored from the OH oxidation of Acenaphthylene

Impact of NO_x on product distributions and SOA formation have been observed

Proposition of identified secondary chemistry in the extended mechanisms

SOA yields in the range 46-68% have been measured

HIGHLIGHTS